POLITECNICO DI TORINO
Repository ISTITUZIONALE

Tantalum-based multilayer coating on cobalt alloys in total hip and knee replacement

Original
Tantalum-based multilayer coating on cobalt alloys in total hip and knee replacement / Balagna, Cristina; Faga, M. G.; Spriano, Silvia Maria. - In: MATERIALS SCIENCE AND ENGINEERING. C, BIOMIMETIC MATERIALS, SENSORS AND SYSTEMS. - ISSN 0928-4931. - 32:(2012), pp. 887-895. [10.1016/j.msec.2012.02.007]

Availability:
This version is available at: 11583/2489298 since:

Publisher:
Elsevier

Published
DOI:10.1016/j.msec.2012.02.007

Terms of use:
openAccess

This article is made available under terms and conditions as specified in the corresponding bibliographic description in the repository

Publisher copyright

(Article begins on next page)

05 May 2023

Tantalum-based multilayer coating on cobalt alloys in total hip and knee replacement

C. Balagna[a,*] , M.G. Faga[b], S. Spriano[a]

This is the author post-print version of an article published on *Materials Science and Engineering: C*, Vol. *32*, pp. *887-895*, *2012* (ISSN *0928-4931*).
The final publication is available at
http://dx.doi.org/ 10.1016/j.msec.2012.02.007
This version does not contain journal formatting and may contain minor changes with respect to the published edition.
The present version is accessible on PORTO, the Open Access Repository of the Politecnico of Torino, in compliance with the publisher's copyright policy.
Copyright owner: *Elsevier*.

[a]*Materials Science and Chemical Engineering Department, Politecnico di Torino, Corso Duca degli Abruzzi 24,10129 Torino, Italy*

[b]*Istituto di Scienza e Tecnologia dei Materiali Ceramici, Consiglio Nazionale delle Ricerche, Strada delle Cacce 73, 10135 Torino, Italy*

[*]*Corresponding author: Tel.:* +39 011 5644668; *Fax* : +39 011 5644699;

E-mail address: cristina.balagna@polito.it

Abstract

Cobalt-chromium-molybdenum (CoCrMo) alloys are widely used in total hip and knee joint replacement, due to high mechanical properties and resistance to wear and corrosion. They are able to form efficient artificial joints by means of coupling metal-on-polymer or metal-on-metal contacts. However, a high concentration of stress and direct friction between surfaces leads to the formation of polyethylene wear debris and the release of toxic metal ions into the human body, limiting, as a consequence, the lifetime of implants.

The aim of this research is a surface modification of CoCrMo alloys in order to improve their biocompatibility and to decrease the release of metal ions and polyethylene debris. Thermal treatment in molten salts was the process employed for the deposition of tantalum-enriched coating. Tantalum and its compounds are considered biocompatible materials with low ion release and high corrosion resistance.

Three different CoCrMo alloys were processed as substrates. An adherent coating of about 1 μm of thickness, with a multilayer structure consisting of two tantalum carbides and metallic tantalum was deposited. The substrates and modified layers were characterized by means of structural, chemical and morphological analysis. Moreover nanoindentation, scratch and tribological tests were carried out in order to evaluate the mechanical behaviour of the substrates and coating. The hardness of the coated samples increases more than double than the untreated alloys meanwhile the presence of the coating reduced the wear volume and rate of about one order of magnitude.

Keyword: CoCrMo alloys, Tantalum coating, Wear resistance, Biocompatibility, Arthroprosthesis

1. Introduction

Hip joint replacement may be performed by means of an ultra high molecular weight polyethylene (UHMWPE) acetabular cup articulating against a metal femoral head. In recent years, the interest in the use of metal-on-metal (MoM) coupling in the treatment of younger and more active patients has increased because it offers lower wear rates and greater longevity. On the other hand, knee joints are usually replaced by an UHMWPE tibial plate coupling with a metal femoral component. Excellent mechanical properties, high corrosion and wear resistance permit the use of cobalt-chromium-molybdenum (CoCrMo) alloys as the material in the prosthetic surgery of these artificial joints [1, 2].

However, devices composed of metal on UHMWPE (MoP) bearing surfaces are subjected to polymer wear and to corrosion of the metallic component, limiting the longevity of the implant. It is well known that polyethylene debris contributes as a principal factor to osteolysis and to implant failure for aseptic loosening. In fact, UHMWPE particles are produced in the size range of biological activation and so an inflammatory response is usually activated. Macrophages phagocytose wear debris after interaction with periprosthetic tissue and then they release cytokines and mediators of inflammation, developing a granulomatous tissue [3-5]. In contrast, metallic debris are smaller in volume and in size than polyethylene debris, but they expose a higher surface area and hence they are more prone to corrosion.

In any case, the corrosion risk of CoCrMo devices is enhanced due to human body fluids and surface friction. Even if Co and Cr are present in human body tissue, an increment of them can cause hypersensitivity and drastic inflammatory reactions [6-8]. In fact released metallic particles and ions can circulate in the human body through blood and lymph and they accumulate in the implant site or in the lymphonodes and liver. Many studies describe the potential toxic behavior of Co and Cr ions, such as Co^{2+}, Cr^{3+} and Cr^{6+}. In particular, Cr is the most hazardous element to human health. Its toxicity is strongly dependent on its valence state [9]. Cr (III) can cause chromosome breakage and DNA damage [7]. Cr (VI) is more dangerous even if less common, but it

is easily capable of reducing itself into more reactive species, such as Cr (III), after entering the cells. It has been verified *in vitro* that the toxicity of Co and Cr is strongly linked to type, concentration and exposure time. The predominant phenomena observed in cells are initially apoptosis, and subsequently necrosis [10]. Moreover, a study, conducted *in vitro* with human osteoblasts, confirmed that Co^{2+} and Cr^{3+} could induce oxidative stress with consequent citotoxicity, influencing cell redox state and stimulating the expression of antioxidant enzymes [11].

In recent years, researchers have focused their attention on another metal, tantalum (Ta), which arose their interest firstly in the bulk form, such as plates and suture wires, and then with a porous structure similar to spongeous bone as the commercial Trabecular Metal ^{TM}, for different orthopaedic applications. Ta has an excellent corrosion resistance [12, 13] and it is considered a biocompatible metal [14]. In fact, it is suitable for cell adhesion, proliferation and differentiation [15-17]. Additionally Ta, or deposited films of Ta oxide and nitride, could be used for cardiac and vascular devices thanks to haemocompatible properties [18, 19]. In the past, protective films enriched in Ta or Ta carbide were deposited by means of magnetron-sputtering or electrochemical deposition from molten salts on steel substrates [20,21] or by means of molten salts on carbon fibers [22].

In the present work, a Ta-rich coating is deposited on CoCrMo alloys through a thermal treatment in molten salts. This technique was patented [23] and it is described in detail in previous works [24, 25]. This method allows a coating composed of Ta carbides and eventually metallic Ta, harder and more biocompatible than the substrate, with a strong and graded interface to be obtained.

2. Material and Method

Three CoCrMo alloys were used as substrates for Ta-coating deposition. Two alloys contained low content of carbon and they were manufactured by wrought procedure (LC-W) or by casting (LC-C), while the other alloy contained a high carbon amount and it was obtained by casting (HC-C). All the samples were supplied by Smith & Nephew Orthopaedics AG. Table 1

summarizes the composition of the alloys. The amount of carbon was analysed by optical spectrometry (Spectro-SpectroLab5), while the other elements were determined by energy dispersion spectrometry (SEM-EDS, Philips 525M). This analysis is affected by an error of about 1 % and it affects mainly the datum about nickel.

A Ta-rich coating was formed on the substrates through a thermal treatment in molten salts, patented by Spriano and Bugliosi [23] and described in previous works [24,25]. Briefly, one sample at a time was subjected to the surface modification. A disk-shape sample, with 30 mm of diameter and 3 mm of thickness, was inserted in a graphite crucible, after weighting and cleaning with acetone, and it was covered with a solid salt mixture contained 98wt.% of K_2TaF_7 powder and wt.2% of metallic Ta powder. This composition was chosen on the base of previous works [24,25]. Then the crucible was introduced into a vertical tubular furnace in order to perform the treatment under argon flux. The sample was cleaned with distilled water and weighted again, after thermal treatment, in order to evaluate the weight increment due to the coating formation. Finally, it was slightly polished with silica colloidal solution, for removing the residual salts on the surface. Tests performed by using different process parameters, in terms of salts amount, isothermal temperature and time at the isothermal temperature, were done in order to set the best condition. The salt mixture quantity varied among 10 and 17 g, while the thermal treatments were carried out at the temperatures among 950-1000°C and the isothermal time among 30-60 minutes. The treated samples are called, in this report, by using an acronyms containing the maximum temperature of the isothermal treatment added to the name of the untreated alloy (such as LC-W970 for the low carbon wrought alloy treated at 970°C).

The crystallographic structure of the bulks and the coatings was investigated using X-ray diffraction (XRD, X'Pert Philips diffractometer) with the Bragg–Brentano camera geometry and the Cu Kα incident radiation. X'Pert High Score software and the PCPDF data bank were used to accomplish the pattern analysis of crystalline phases. Moreover parallel beam XRD (PB-XRD) measurements with incident angle fixed at 1° mainly permitted the evaluation of the crystalline

phase of the modified layer. The percentage quantity of one phase ($\%phaseA$) was calculated with the following ratio:

$$\%phaseA = \frac{\sum I_{peaksA}}{\sum I_{peaksTot}} * 100 \quad (1)$$

where A was the considered phase, $\sum I_{peaksA}$ was the sum of the intensities of peaks belonged to the considered phase, $\sum I_{peaksTot}$ was the sum of the intensities of all peaks belonged to all phases detected from diffractograms.

The composition of the substrates and the treated alloys, as well as the coating morphology and the thickness were investigated by Scanning Electron Microscopy and Energy Dispersion Spectrometry (SEM-EDS, Philips 525M) at two different voltages, 15 and 30 kV.

In addition, the coating thickness was analysed by Calotest. A stainless steel ball with a diameter of 20 mm rotated for 30 minutes in contact with the sample surface, under a fixed load and an abrasive slurry. This procedure allowed the erosion of the coating, obtaining a crater which was analysed then by means of SEM (using back scattered electrons).

A profilometer (Tencor P-11) measured the disk roughness in terms of Ra (arithmetical mean roughness), Rq (root mean square value) and Rz (ten-point mean roughness).

The nanoindentation test was performed with a nanoindenter (Nano Indenter ® XP of MTS System Corporation). A normal load of 10 mN was applied, reaching a maximum depth of indentation of 300 nm, thus avoiding the substrate influence.

The friction coefficient of the treated and the untreated disks was extracted from a pin on disc test using a CSEM high temperature tribometer, with a reticulate polyethylene pin. Test parameters were the normal load of 7 N, the linear speed of 10 cm/s and the laps number of 10000. The circumference radius was fixed during the whole test, but it varied between 4-10 mm among the different analysis. Moreover the HC-C sample was undergone to a ball on disc test, with an alumina ball, in order to evaluate the wear behaviour and to simulate a hard-hard coupling. In this

case, instrument and conditions were the same used for pin on disc test, only enhancing the number of laps to 25000. The wear rate (mm^3/Nm) was calculated dividing the wear track volume for the product between the applied load and the sliding distance. The sliding distance was the number of laps multiplied for $2\pi r$, where r was the radius of the track circumference. The wear track profile was evaluated by means of the profilometer. Both tests were performed at the human body temperature (37°C) in a wet environment using the dilute bovine serum as lubricant. The dilute bovine serum was prepared as a solution of 25% vol. of calf bovine serum and 75%vol. of distilled water with the addition of Na_3N as an antibacterial agent in the ratio of 1g/l.

The adhesion between coating and substrate was evaluated by means of a scratch test performed with a commercial CSEM Revetest provided with detectors of friction force and acoustic emission. Each sample was tested with three measurements, using a Rockwell C diamond stylus with 200 μm of radius that produced a line scratch (4.91 mm long) under a normal load continuously increasing up to a maximum value of 100 N. The loading rate had a range between 50 and 200 N/min with a speed of 10 mm/min. Normal load, friction force and acoustic emission were recorded during the tests. The minimum critical load was difficult to be properly estimated by acoustic emission, thus a combination of the acoustic emissions and the reflected light microscope was used in order to determine it.

3. Results and discussion

3.1 CoCrMo alloys as substrates

The three CoCrMo alloys, used as substrates, differed with regards to the manufacturing technology (plastic deformation or casting), their composition and their carbon content (table 1). The carbon quantity decreased from HC-C, to LC-C and then to LC-W alloy, whose value was so low (under 0.01 wt.%) that the optical spectrometer was not able to measure it.

Less metallic carbides (Mo or Cr carbides) were present inside the LC alloys, compared to the HC one, because of their low carbon amount, decreasing the hardness and mechanical properties

of the bulk. These alloys are usually used for hip (LC-W) and knee artificial joints in MoP coupling, where the frictional regime is not as severe as it is in MoM coupling. HC-C was analysed in this work because it is suitable both for MoM and MoP bearing.

3.2 Thermal treatment optimization

Ta-based coating was deposited on the LC-W, LC-C, HC-C surfaces by means of the thermal treatment in molten salts through a mechanism of diffusion. It was fundamental to optimize the process in order to avoid corrosion of the substrate, which happens in too severe conditions. For this purpose, the isothermal temperature and time, as well as the salt quantity were set case by case. The weight increment of samples, after surface modification, was verified as a preliminary characteristic for the selection of the process parameters and for a first evaluation of the amount of Ta-enrichment. Two different isothermal temperatures (970 and 990 °C) were chosen because it was observed that layers with different properties were deposited on the substrates under these conditions. A graph relative to the weight increment obtained after a series of tests at the two temperatures (970 and 990°C) performed on LC-W is reported in Figure 1. In this case, the salt quantity was fixed at 17 g and 12,75 g for low and high temperatures, respectively. The isothermal time ranged from 30 to 60 minutes. The highest bar of the histogram (45 min) represents the maximum weight increment and thus the optimized parameters, while the Ta-enrichment is the lowest at the shortest time and corrosion occurred at the longest time.

Table 2 summarizes the optimized process parameters for each substrate. The quantity of salts, used for casting alloys, LC-C and HC-C, was less than that used for the wrought alloy substrate (LC-W) because of their proneness to corrosion, which imposed less severe conditions. LC-C990 was characterized by the maximum weight increment (32 mg).

3.3 Crystallographic analysis

XRD analysis relative to the untreated and treated alloys is reported in Figure 2. The substrates were characterized by the presence of two crystalline structures of cobalt, cubic (FCC Co, PCPDF reference code 01-089-4307) and hexagonal phase (HCP Co, PCPDF reference code 01-089-4308) (Fig. 2a). The wrought alloy (LC-W) contained a lower amount of the HCP phase, about 1%, with respect to the cast alloys, and a random orientation of crystals, corresponding to an annealed condition. Instead the diffractograms of LC-C and HC-C showed a higher amount of the hexagonal cobalt phase, 29 and 32% respectively, and a preferential orientation of the FCC phase, according to the as-cast condition. The peak width revealed finer crystals in the cast samples than in the wrought one.

Deposited coating was composed principally of Ta carbides (Fig. 2b-c). In particular, the process formed tantalum carbide (TaC, PCPDF reference code 00-035-0801) on all the treated samples and a second phase of emi-tantalum carbide (Ta_2C, PCPDF reference code 00-018-1296) observable in all the disks treated at 970°C and LC alloys treated at 990°C. HC-C990 represented an exception because no Ta_2C peaks were detected. Finally, some peaks belonging to the substrate were noticed with an increment of the HCP Co phase with respect to the untreated samples in some cases. They were less intense on the LC alloy (treated at 970 or 990°C).

Parallel beam XRD diffractograms of the treated disks are reported in Figure 3 for a better evaluation of the crystalline structures and the layer distribution. The diffractograms relative to LC-W970 and HC-C970 showed a similar trend. The coatings of all the alloys treated at 970°C (Fig. 3a) contained both Ta_2C and TaC and a variable amount of a third phase, consisting of the metallic hexagonal tantalum (HCP Ta, PCPDF reference code 01-089-1545). Maybe, the HCP Ta formed the most external layer of the modified surface and it was too thin to be detectable by Bragg Brentano analysis. Although Ta is usually a cubic phase, its crystalline structure, in this case, was hexagonal, probably because of a crystallographic correlation with the hexagonal structure of the closest layer of Ta_2C. Furthermore, it is deducible that Ta_2C formed an intermediate layer between

Ta and TaC, evaluating the increment/decrement of the relative intensities of Ta_2C/TaC peaks with respect to the same patterns obtained by the Bragg Brentano diffractograms. The external Ta layer was thicker in the case of LC-C970. Also a weak cobalt peak belonged to the substrate was marked on all PB-XRD patterns.

The external coating on HC-C990 and LC-W990, detected by PB-XRD, was composed only of the TaC phase. On the contrary, the coating on LC-C990 presented the three layers, typical of the sample treated at the lowest temperature.

Table 3 reports the percentage quantities of the phases in the coatings, calculated by means of (1), considering the PB-XRD diffractograms . The coatings obtained at 970°C showed quantities of TaC and Ta_2C similar with a prevalence of Ta_2C in the low carbon alloys. An higher amount of Ta (3%) was detected for both the LC-C substrates, treated at 970 and 990°C.

Hence, it can be stated that the thermal process enabled the diffusion of the Ta from the salt mixture into the substrate where it was able to react with carbon until forming a coating with different layers in succession, from the most internal TaC, to the intermediate Ta_2C and finally to the most external Ta. In this way, a progressive increment in Ta and decrement in carbon was obtained moving away from the substrate. The presence of a single layer coating on LC-W990 and HC-C990 and the multilayer structured coating on LC-C990 revealed by PB-diffraction (Fig.3b) could be explained considering two aspects, the process temperature and the carbon amount in substrate. In fact, a higher temperature is able to increase the reactivity between carbon and Ta and to speed up the diffusion rate of the atoms forming more TaC phase. Moreover, HC-C offered a higher carbon amount, thus the formation of a layer of a carbon-rich phase, such as TaC, was easier. The LC-C alloys showed higher amount of Ta-rich phases, in particular the Ta after the treatment at 970°C and the Ta_2C after the treatment at 990°C. The LC-W substrate, in spite of the low carbon content, behaved differently probably because of its high molybdenum content and different carbides stability and microstructure.

An XPS analysis, reported in a previous work [25], confirmed the formation of this multilayer structure, depending principally on the treatment temperature.

3.4 Morphological and compositional analysis

The microphotographs obtained by means of back-scattering SEM analysis are reported in Figures 4 and 5 for evaluating coatings morphology and thickness. As it can be seen in Figure 4, all the coatings completely recover surfaces without cracks and pores, following the substrates profiles. The coating thickness of LC-W990 was about 400-500 nm and thinner than LC-C970 (600-700 nm) in accordance with the weight increment measurement (table II) and with the XRD analysis (Fig. 2b,c). In fact, the peaks of the Co phase belonged to the LC-W990 substrate had higher relative intensity.

Figure 5 reports BS-SEM images relative to the cross section and the ball crater, obtained by Calotest, on LC-C990. This sample got attention for its different properties compared to the others. In fact, although it was subjected to a thermal treatment at 990°C, its coating was measured as thicker than the other samples and it reached a value of 1 μm, explaining the elevated registered weight increment, the presence of weak Co peaks in XRD diffractogram (Fig. 2c) and the multilayer structure (Fig.3b). The latter was also well visible by observing the photo of the ball crater (Fig. 5b), where the most external and the lightest circle could be attributed to Ta_2C layer, while the innermost grey could be referred to TaC.

A graphical scheme of the different coatings is drawn in Figure 6 in order to summarize their structure and thickness.

Data acquired from EDS quantitative analysis are summarized in the histogram reported in Figure 7. The weight percentage of Ta reached values from 90 until almost 97 wt.% on the coatings, meanwhile Co and Cr decreased drastically and Mo was not detected anymore on any alloys. According to the weight increment (Table 2) and the thickness of the coatings (Fig. 6), LC-C990

showed the highest value of Ta and the lowest quantity of Co, meanwhile LC-W970 had the lowest Ta amount.

Surface roughness is an essential property for materials subjected to wear and used in artificial joints. It is well known that a roughness (Ra) on the order of few nanometers permits wear and friction to be reduced. Commercial MoP and MoM total replacement hip joints have a roughness of 5-15 nm. They operate in the mixed lubrication regime, with a load transmission supported partly by the asperity contacts and partly by a hydrodynamic action, while higher roughness values can induce a deleterious boundary lubrication regime. Table 4 reports the roughness data in terms of Ra, Rq and Rz measured on the untreated and the treated samples. Values of the untreated samples refer to a mirror polished surface. The roughness underwent a moderate increment after the coating formation, achieving a maximum value of about 12 nm (HC-C990), anyhow acceptable according to the international standard on metallic articulating surface [26].

3.5 Mechanical properties

Table 5 summarizes data extracted from the nanoindentation test performed with a maximum load of 10 mN both on the treated and the untreated alloys. The examined parameters were the nanohardness, the Young's modulus and the indentation depth. Considering the coating thickness, it could be concluded that the indentation depth never reached the substrates. An important increment of the nanohardness and the Young's modulus was verified due to the presence of the coating. However, it was difficult to understand at what kind of layer among TaC, Ta_2C and Ta, the nanohardness was relative. In fact, no many differences between thermal treatments at 970 and 990°C were noticed. The most elevate hardness and the elastic modulus were achieved for the processed LC-C alloys, in particular for LC-C990. Probably a thicker coating influenced and enhanced this parameter.

3.6 Tribological properties

The friction coefficient between a reticulate polyethylene pin and the metal disk was the same for all untreated alloys and equal to 0.1. The presence of the coating slightly influenced and decreased it, but the friction coefficient was not sensitive to the different crystalline structures of the external layer.

On the contrary, the treated HC-C alloys showed a significant increment of the wear resistance compared to the substrate as it could be observed in the graph relative to the sections of the wear tracks profile reported in Figure 8. The wear resistance of this alloy was tested because, as described in the introduction, it is of interest for hard-on-hard coupling such as MoM. The coating was able to reduce wear volumes and rates of one order of magnitude and they decreased the track depths from about 3 to less than 1 μm. The structure of the modified surface seemed not to influence the wear resistance. Wear mechanism of this kind of alloy was well studied in the previous work [25]. Abrasion was the principal cause of the wear in the substrate and a contribution of third body damage was also revealed because of the metal carbides inside matrix. The Cr and Mo carbides were able to crack and pull-out and they acted such as third body of very hard nature even if they were few and isolated for the casting manufacturing process. The same mechanism was observed in the treated alloys where the passage of the alumina ball removed the external layer of the coating and it spread the abrasive particles of tantalum carbides inside the track.

3.7 Adhesion test

The critical loads of the scratch test were assessed by the track observation via optical microscope, with the help of acoustic emission signals. Figure 9 shows the whole track left by the scratch indenter on the 970 treated-samples. For LC samples, first cracks appeared in the range 7-9 N for wrought alloy and 11-16 N for the casting one. They were ascribable to buckling type, which are typically produced by interfacial defects in response of comprehessive stress occurring ahead of the indenter [27].

In the case of the LC-W970 sample, only the buckles appeared at about 9N (Fig.10a) instead the first observable cracks in the scratch track of LC-C970 were chevron-type (Fig. 11a), occurring at 11N ca., while the buckling cracks were noticed only at 15N (Fig.11b), indicating a higher adhesion between the coating and the substrate for this sample. The starting of the coating delamination was at about 30 N for LC-W970 (Fig.10c) and LC-C970 (Fig.11c). Instead a lower load was needed in the case of the samples treated at the highest temperature (14 N for LC-W990 and 22 N for LC-C990) for beginning the delamination. It occurred by cracking at the edge of the scratch track while delamination inside the track appeared at higher load (about 40 N). The HC samples behaved worst than LC substrates with a lower critical load.

The HC-C970 sample revealed the same mechanism of LC-C970, with the appearance firstly of the chevron-type cracks at about 6 N (Fig.12a) and, then, of the buckles at 13 N (Fig.12b). Finally, the delamination phenomena started at about 25 N (Fig.12c). The HC-C990 sample, composed of a single layer of TaC, showed delamination at a quite low load (11N) without the appearance of the buckling or chevron type cracks, so it had the worst scratch resistance (Fig.13). Hence, it can be concluded that all the LC treated alloys presented the same resistance to a first damage, while the HC treated alloy was less resistant. The delamination resistance was higher in the case of the LC alloys treated at 970°C, characterized by the multilayer structure and a higher thickness of the coating. On the contrary, the samples presenting only a monolayer coating of TaC had worse scratch resistance.

3.8 Final considerations

This coating, with a thickness less than 1 μm, will probably not resist to the wear to which an implant for the substitution of joints is usually subjected throughout its lifetime. However, this work could be considered an essential starting point for evaluating any improvement in the tribological behaviour of the material, due to the coating formation by means a thermal treatment

and its adhesion to the substrate. Anyway, an increment of the coating thickness will be necessary for the real applications.

In addition, the corrosion behaviour of the samples will be deeply evaluated in the future, considering that this material is usually in direct contact for long time with corrosive human body fluids. In previous work [24], the measurements of the metal ions, released into the dilute bovine serum during the wear test, were carried out demonstrating a relevant decrement of the metal ion content into the solution due to the presence of Ta coating which acted as a barrier.

4. Conclusions

In this work, a coating on three different CoCrMo alloys, with high and low carbon content, was obtained by means of a thermal treatment in Ta molten salts. Process parameters, such as isothermal temperature and time, as well as salts amount, were optimized case by case.

The deposited coating was continuous and homogeneous and it was formed by a multilayer structure of tantalum carbides (TaC and Ta_2C) and eventually a third external layer of metallic tantalum (HCP Ta). The thermal treatments carried out at higher temperature and on high carbon content substrate were able to deposit more frequently a single layer of TaC. Roughness showed a moderate increment considering acceptable for the ultimate purpose.

The modified surface increased the hardness of the samples more than double with respect to the untreated alloys. In addition, the wear resistance was prominently improved and the coating, formed during the thermal treatment, is able to reduce the wear volume and rate of about one order of magnitude. However, it seemed to not influence the friction with polyethylene.

Finally, the coating adhesion depended on its structure and on the carbon content of the substrate. In fact, the samples of LC alloys treated at 970°C showed higher critical loads because of their multilayer structure.

Acknowledgement

Authors would like to thank Smith & Nephew Orthopaedics AG that contributed to the realization of this study with the supply of CoCrMo alloys analysed in this work.

References

[1] A. Marti, Cobalt-based alloys used in bone surgery, Injury, Int. J. Care Injured 31 (2000) S-D18-21

[2] M. Niinomi, Recent metallic materials for biomedical applications, Metall. Mater. Trans. A, 33A (2002) 477-486

[3] E. Ingham, J. Fisher, The role of macrophages in osteolysis of total joint replacement, Biomater. 26 (2005) 1271-1286

[4] E. Ingham, J. Fisher, Biological reactions to wear debris in total joint replacement, Proc. Instn Mech. Engrs part H 214 (2000) 21-37

[5] R.K. Sethi, M.J. Neavyn, H.E. Rubash, A.S. Shanbhag, Macrophage response to cross-linked and conventional UHMWPE, Biomater. 24 (2003) 2561-2573

[6] D. Granchi, E. Cenni, D. Tigani, G. Trisolino, N. Baldini, A. Giunti, Sensitivity to implant materials in patients with total knee arthroplasties, Biomater 29 (2008) 1494-1500

[7] A.G. Cobb, T.P. Schmalzreid, The clinical significance of metal ion release from cobalt-chromium metal-on-metal hip joint arthroplasty, Proc. Instn Mech. Engrs part H 220 (2006) 385-398

[8] D. Granchi, G. Ciapetti, S. Stea, L. Savarino, F. Filippini, A. Sudanese, G. Zinghi, L. Montanaro, Cytokine release in mononuclear cells of patients with Co-Cr hip prosthesis, Biomater. 20 (1999) 1079-1086

[9] Y. Okazaki, E. Gotoh, Comparison of metal release from various metallic biomaterials in vitro, Biomater. 26 (2005) 11-21

[10] I. Catelas, A. Petit, H. Vali, C. Fragiskatos, R. Meilleur, D.J. Zukor, J. Antoniou, O. L. Huk, Quantitative analysis of macrophage apoptosis vs. necrosis induced by cobalt and chromium in vitro, Biomater. 26 (2005) 2441-2453

[11] C. Fleury, A. Petit, F. Mwale, J. Antoniou, D.J. Zukor, M. Tabrizian, O. L. Huk, Effect of cobalt and chromium ions on human MG-63 osteoblasts in vitro: Morphology, cytotoxicity and oxidative stress, Biomater. 27 (2006) 3351-3360

[12] M.D. Bermudez, F. J. Carrion, G. Martınez-Nicolas, R. Lopez, Erosion–corrosion of stainless steels, titanium,tantalum and zirconium, Wear 258 (2005) 693–700

[13] A. Robin, J. L. Rosa, Corrosion behavior of niobium, tantalum and their alloys in hot hydrochloric and phosphoric acid solutions, Int. J. Refract. Met. & Hard Mater. 18 (2000) 13-21

[14] B.R. Levine, S. Sporer, R.A. Poggie, C.J. Della Valle, J.J. Jacobs, Experimental and clinical performance of porous tantalum in orthopaedics surgery, Biomater. 27 (2006) 4671-4681

[15] D.M. Findlay, K. Welldon, G.J. Atkins, D.W. Howie, A.C.W. Zannettino, D. Bobyn, The proliferation and phenotypic expression of human osteoblasts on tantalum metal, Biomater. 25 (2004) 2215-2227

[16] T.A. Schildhauer, E. Peter, G. Muhr, M. Koeller, Activation of human leukocytes on tantalum trabecular metal in comparison to commonly used orthopaedic metal implant materials, J. Biomed. Mater. Res. A 88 (2) (2009) 332-341

[17] K.J. Welldon, G.J. Atkins, D.W. Howie, D.M. Findlay, Primary human osteoblats grow into porous tantalum and maintain an osteblastic phenotype, J. Biomed. Mater. Res. A 84(2) (2007) 691-701

[18] Y.X. Leng, J.Y. Chen, P. Yang, H. Sun, J. Wang, N. Huang, The biocompatibility of the tantalum and tantalum oxide films synthesized by pulse metal vacuum arc source deposition, Nucl. Instn. Meth. Phys. Res. B 242 (2006) 30-32

[19] Y.X. Leng, H. Sun, P. Yang, J.Y. Chen, J. Wang, G.J. Wan, N. Huang, X.B. Tian, L.P. Wang, P.K. Chu, Biomedical properties of tantalum nitride films synthesized by reactive magnetron sputtering, Thin Solid Films 398-399(2001)471-475

[20] L. Gladczuk, A. patel, C. S. Paur, M. Sosnowski, Tantalum films for protective coatings of steel, Thin Solid Films 467 (2004) 150-157

[21] S.L. Lee, M. Cipollo, D. Windover, C. Rickard, Analysis of magnetron-sputtered tantalum coatings versus electrochemically deposited tantalum from molten salt, Surf. Coat. Technol. 120-121(1999) 44-52

[22] Z.J. Dong, X.K. Li, G.M. Yuan, Y. Cong, N. Li, Z.J. Hu, Z.Y. Jiang, A. Westwood, Fabrication of protective tantalum carbide coatings on carbon fibers using a molten salt method, Appl. Surf. Sci. 254(2008) 5936-5940

[23] S. Spriano, S. Bugliosi, Medical prosthetic devices presenting enhanced biocompatibility and wear resistance, based on cobalt alloys and process for their preparation, WO 2006/038202A2

[24] S. Spriano, E. Vernè, M.G. Faga, S. Bugliosi, G. Maina, Surface treatment on an implant cobalt alloy for high biocompatibility and wear resistance. Wear 259 (2005), 919-925

[25] C. Balagna, S. Spriano, M.G.Faga, tantalum based thin film for wear resistant arthroprosthesis, J. Nanosci. Nanotechnol. in press, doi:10.1166/jnn.2011.3453

[26] Implants for surgery -- Partial and total hip joint prostheses -- Part 2: Articulating surfaces made of metallic, ceramic and plastics materials, ISO-7206-2.

[27] S.J. Bull. Failure mode maps in the thin film scratch adhesion test, Tribol. Int. 30 (1997) 491-498

Figures

Fig.1. Graph reporting weight increment obtained for treatments performed at 970°C-17g of salts and 990°C-12.75g of salts, varying time of isothermal temperature.

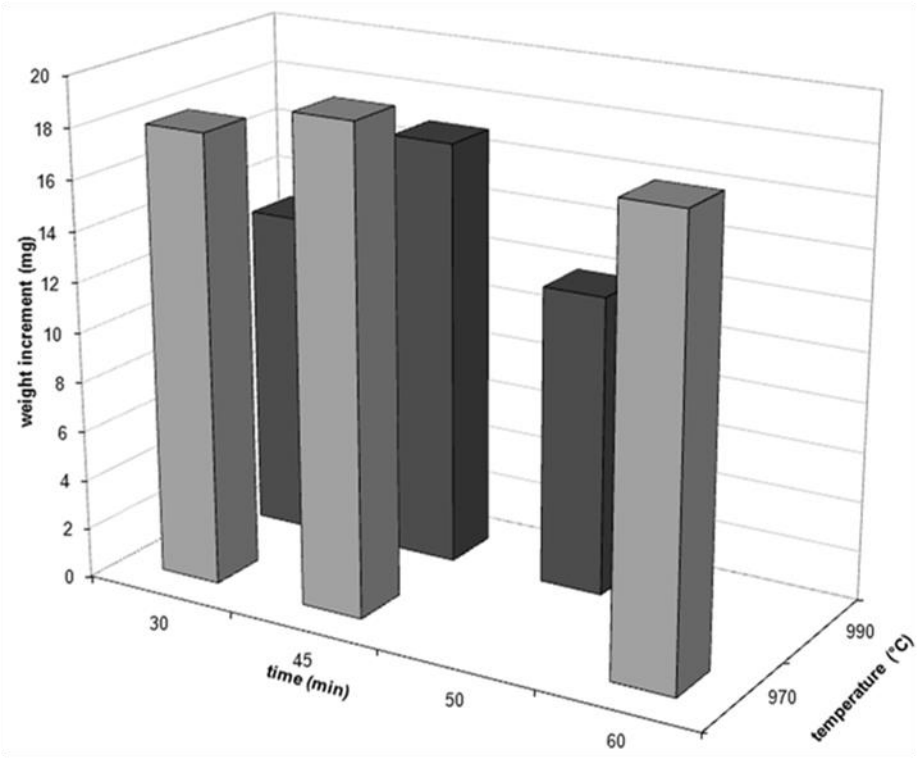

Fig.2. XRD analysis of (a) untreated substrates, (b) 970-treated and (c) 990-treated samples

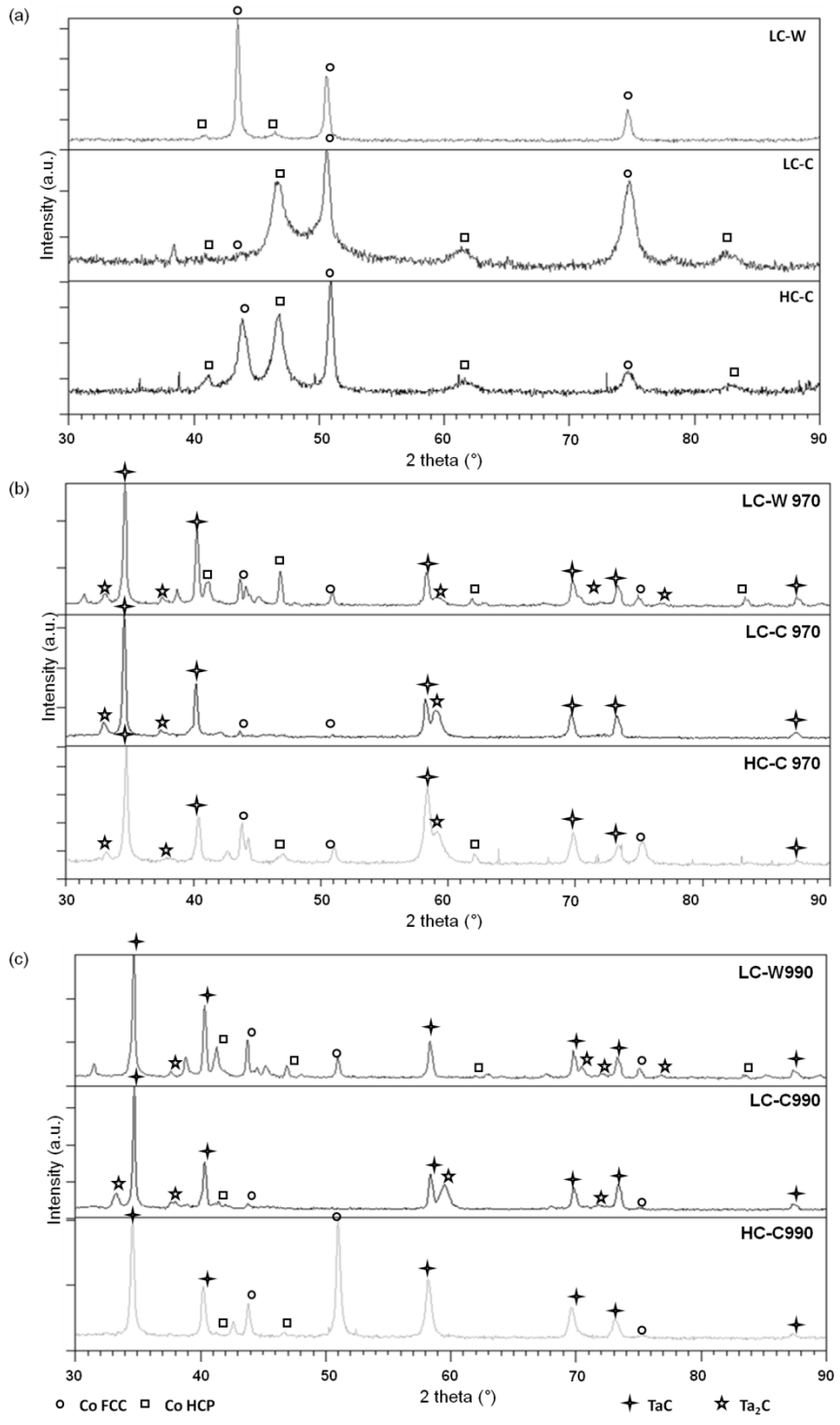

Fig. 3. Parallel beam XRD analysis on the treated sample at (a) 970° C and (b) 990 °C (b)

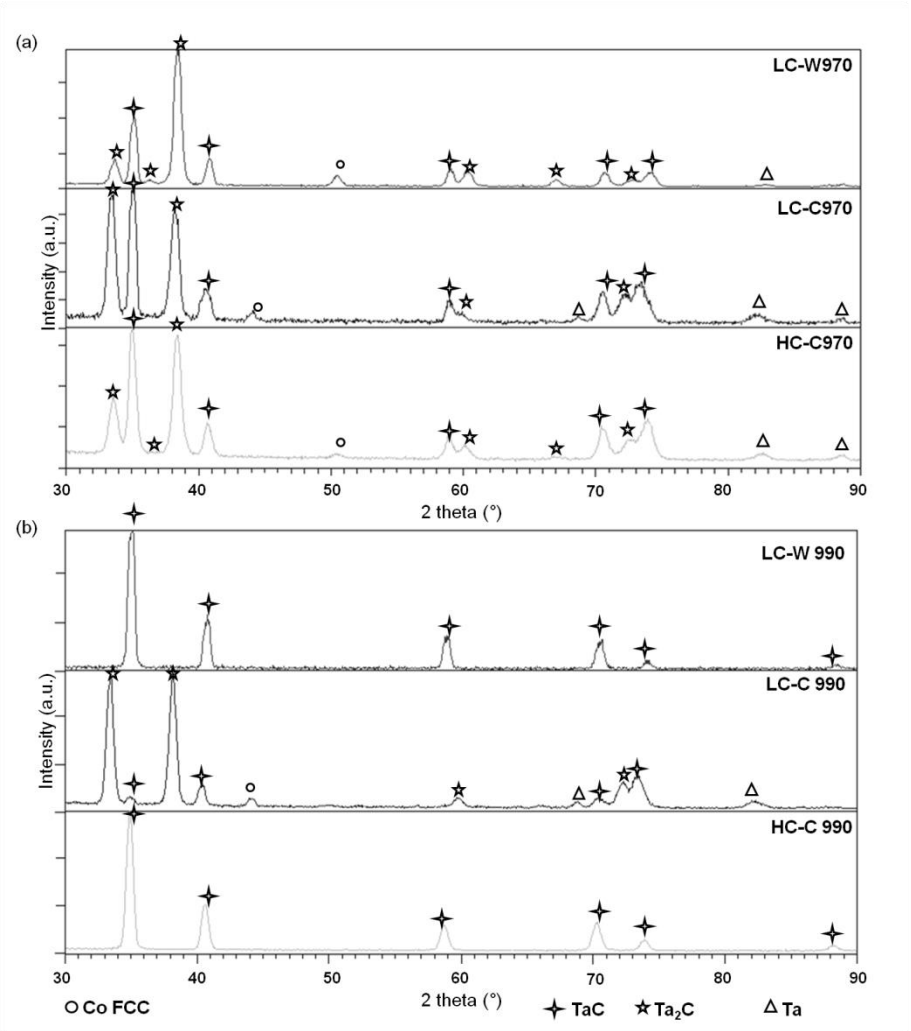

Fig. 4. BS-SEM microphotograph of section samples (a) LC-C970 and (b) LC-W990

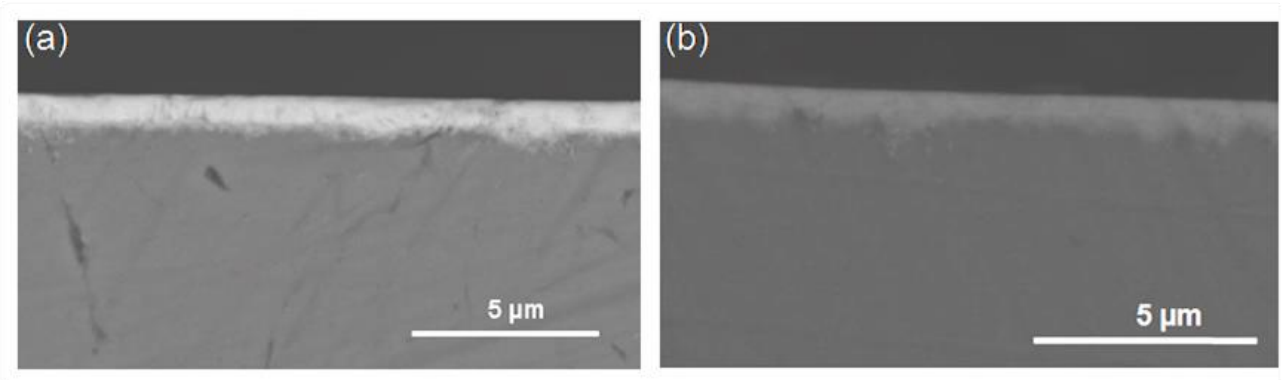

Fig. 5. BS-SEM microphotograph relative to (a) cross section and (b) ball craters on LC-C990

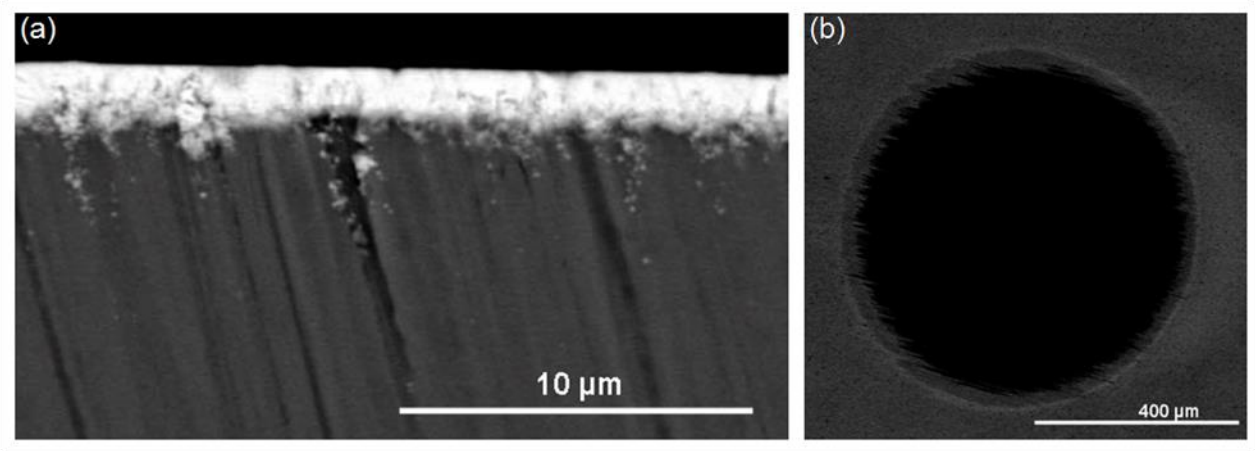

Fig.6. Graphical scheme of samples structure

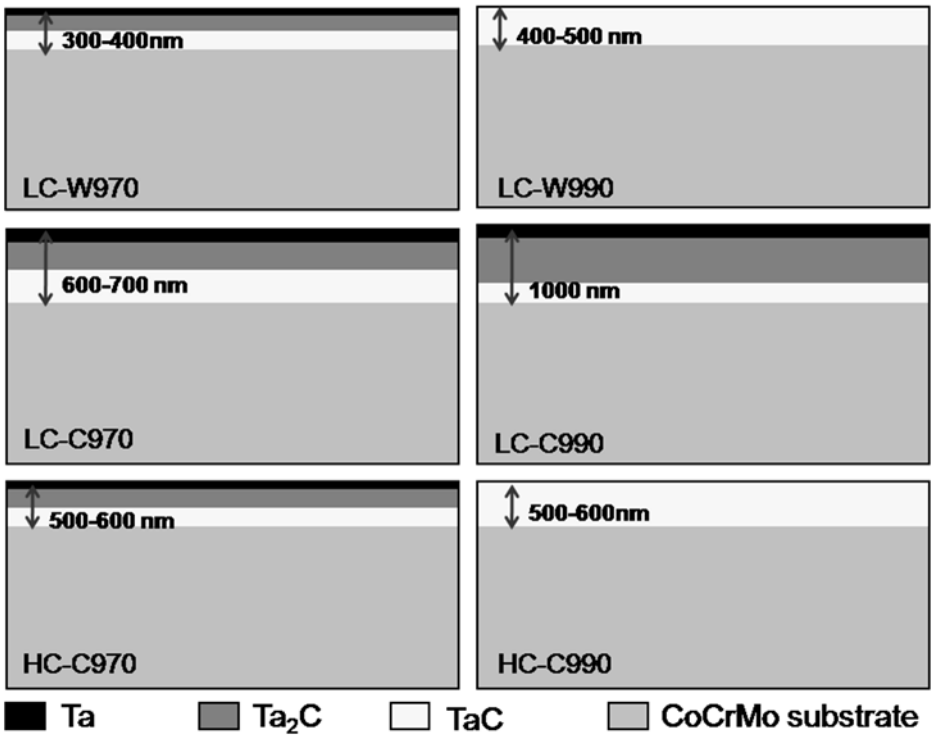

Fig.7. EDS analysis (15kV) on the LC-W, LC-C and HC-C alloys

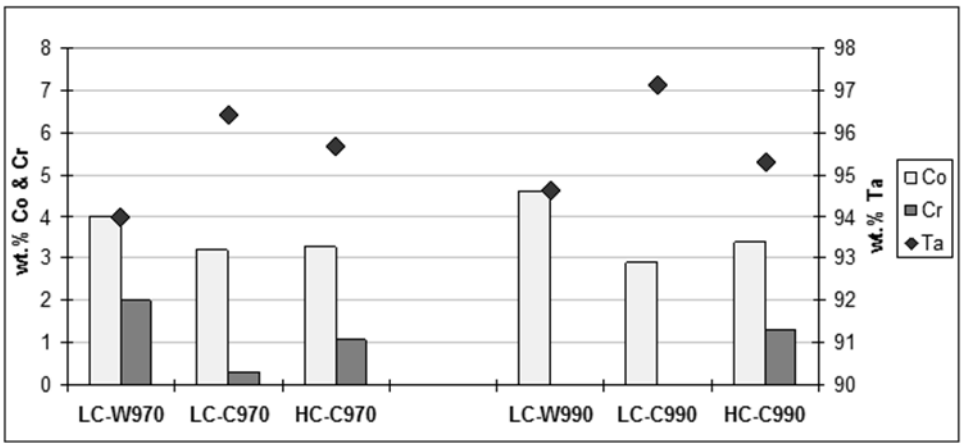

Fig.8. Comparison of track profiles of untreated and treated HC-C alloys

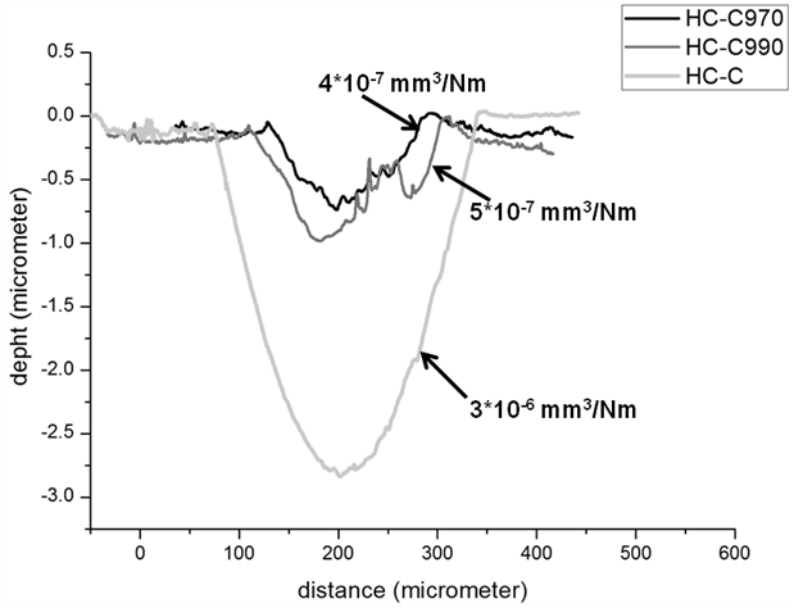

Fig.9. Scratch test signature left by the indenter on samples (a) LC-W970, (b) LC-C970 and (c) HC-C970

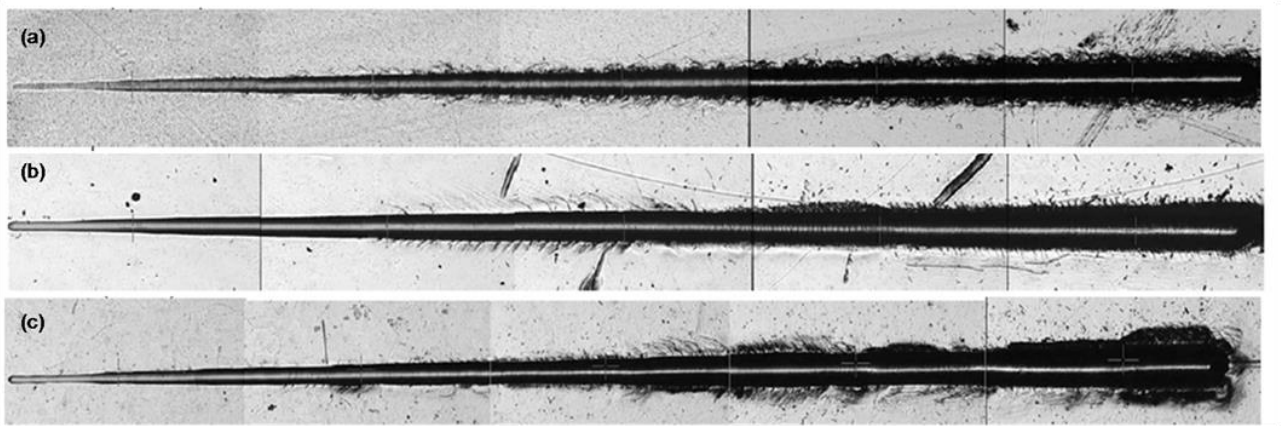

Fig.10. Scratch test result for the sample LC-W970: (a) appearance of buckling type cracks (8.58N); (b) cracks propagation (14.97 N); (c) delamination beginning (30.49N)

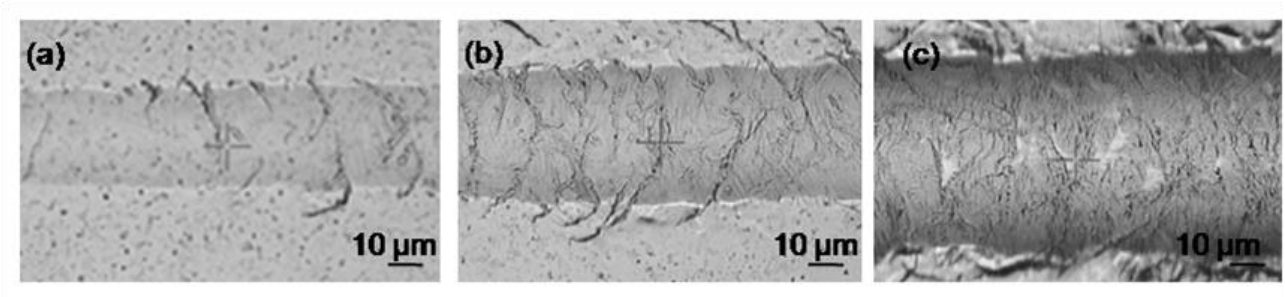

Fig.11. Scratch test result for the sample LC-C970: (a) appearance of chevron type cracks (11.05N); (b) appearance of buckling type cracks (15.16 N); (c) delamination beginning (44.81N)

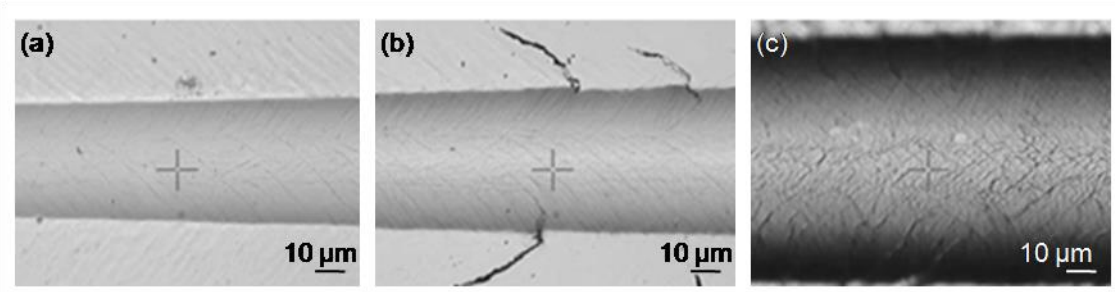

Fig.12. Scratch test result for the sample HC-C970: (a) appearance of chevron-type cracks (6N); (b) buckling type cracks (13N) ; (c) delamination beginning (25N)

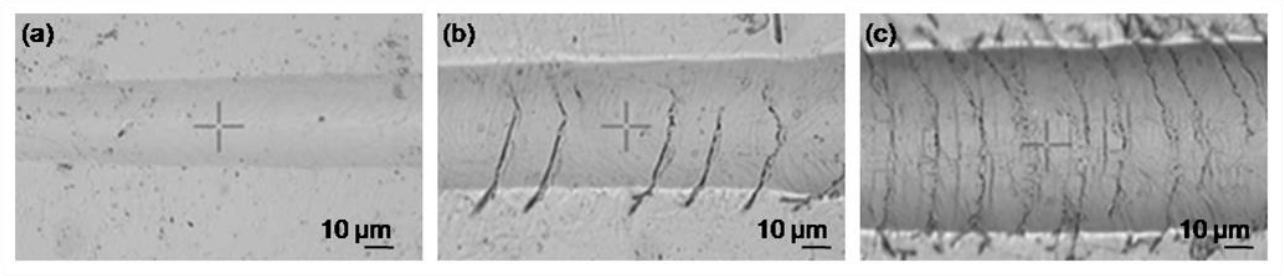

Fig.13. Scratch test result for the sample HC-C990 (a) at load of 6 N and (b) at beginning of delamination at 11 N

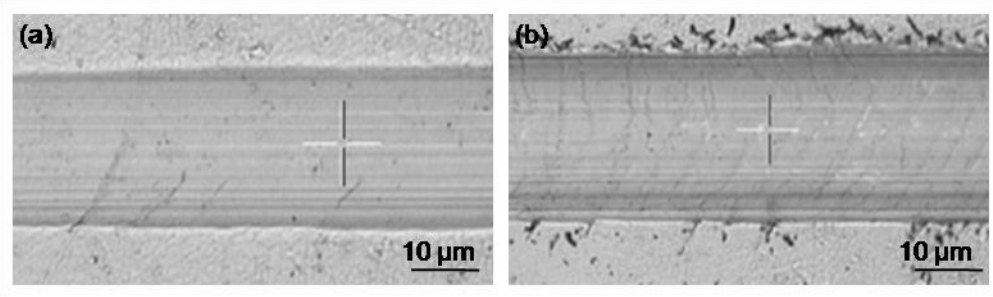

Tables

Table 1
Element composition of analyzed CoMoCr alloys

	EDS analysis				Quantometer analysis
	%wt. Co	%wt Cr	%wt Mo	%wt Ni	%wt C
LC-W	65.0	29.0	5.8	0.2	< 0.01
LC-C	64.1	33.5	2.4	-	0.07
HC-C	66.2	29.8	3.9	0.1	0.20

Table 2
Parameters of the different thermal treatments and weight increment after each process

Sample	Temperature [°C]	Time [min]	Salts [g]	Weight increment [mg]
LC-W	970	45	17	19
	990	45	12.75	17
LC-C	970	45	12.75	21
	990	45	10	32
HC-C	970	45	12.75	24
	990	45	10	18

Table 3
Percentage volume quantity of phases in the coating extracted from parallel beam XRD analysis

	%vol. Ta	%vol.Ta_2C	%vol. TaC
LC-W970	1	59	40
LC-C970	3	51	45
HC-C970	2	45	52
LC-W990	-	-	100
LC-C990	3	79	16
HC-C990	-	-	100

Table 4
Roughness of treated and untreated disks

	Ra (nm)	Rq (nm)	Rz (nm)
LC-W	6 ± 1	6 ± 1	28 ± 2
LC-W970	10 ± 1	12 ± 1	61 ± 4
LC-W990	6 ± 1	8 ± 1	39 ± 3
LC-C	3 ± 2	4 ± 2	25 ± 10
LC-C970	5 ± 1	7 ± 1	34 ± 4
LC-C990	8 ± 1	11 ± 2	70 ± 2
HC-C	6 ± 1	9 ± 1	60 ± 6
HC-C970	11 ± 1	15 ± 2	79 ± 15
HC-C990	12 ± 1	17 ± 1	103 ± 10

Table 5
Nanoindentation values of untreated and treated samples under normal load of 10 mN

Sample	H (GPa)	E (GPa)	Indentation depth (nm)
LC-W	9 ± 1	263 ± 11	230
LC-W970	24 ± 2	263 ± 13	125
LC-W990	25 ± 2	250 ± 12	120
LC-C	9 ± 1	256 ± 10	235
LC-C970	34 ± 4	306 ± 9	125
LC-C990	37 ± 5	316 ± 17	120
HC-C	12 ± 1	250 ± 8	220
HC-C970	27 ± 3	265 ± 18	160
HC-C990	23 ± 2	254 ± 15	180